# Numerical approximation of solitary waves of the Benjamin equation

## V. A. Dougalis

*Mathematics Department, University of Athens, 15784, Zographou, Greece. E-mail: doug@math.uoa.gr*

*Institute of Applied and Computational Mathematics F.O.R.T.H. 71110, Heraklion, Greece. E-mail: dougalis@iacm.forth.gr*

## A. Durán

*Department of Applied Mathematics, University of Valladolid, Campus Miguel Delibes, P/ Belen 15 E-47011 Valladolid, Spain. E-mail: angel@mac.uva.es*

## D. E. Mitsotakis

*Institute for Mathematics and its Applications University of Minnesota 114 Lind Hall 207 Church Street SE Minneapolis MN 55455. E-mail: dmitsot@gmail.com*

**Abstract**

This paper presents several numerical techniques to generate solitary-wave profiles of the Benjamin equation. The formulation and implementation of the methods focus on the approximation of the nonlocal term and the use of numerical continuation algorithms. For solving the attendant nonlinear systems, a comparative study of the performance of such algorithms is made. The paper also explores the generation of multipulse solitary waves with these methods.

*Key words:* Benjamin equation, numerical computation of solitary waves, numerical continuation
*2000 MSC:*

## 1. Introduction

The goal of this paper is the description and comparison of some techniques to compute solitary-wave profiles of the Benjamin equation

$$u_t + \alpha u_x + \beta u u_x - \gamma H u_x - \delta u_{xxx} = 0, \tag{1}$$

In (1), $\alpha, \beta, \gamma, \delta$ are nonnegative constants and $H = \mathcal{H}\partial_x$, where $\mathcal{H}$ denotes the Hilbert transform

$$\mathcal{H}f(x) = \frac{1}{\pi} P.V. \int_{-\infty}^{\infty} \frac{f(y)}{x-y} dy.$$

The Fourier symbol of the operator H is

$$\widehat{(\mathrm{H}u)}(\xi) = |\xi|\widehat{u}(\xi).$$

Particular cases of (1) are the Korteweg-de Vries (KdV) equation ($\gamma = 0, \delta > 0$) and the Benjamin-Ono (BO) equation ($\gamma > 0, \delta = 0$). Equation (1) arises in the study of unidirectional propagation of long internal waves of small amplitude at the interface of two ideal fluids (the heavier of which has infinite depth) in the presence of surface tension [4, 5, 6, 2]. Global well-posedness in $L^2$ for the corresponding initial-value problem is proved in [22], (where other results concerning generalized versions of (1) are also obtained). It is well known that the functionals [5]

$$
\begin{align}
C(u) &= \int_{-\infty}^{\infty} u\, dx, \tag{2}\\
I(u) &= \frac{1}{2}\int_{-\infty}^{\infty} u^2\, dx, \tag{3}\\
E(u) &= \alpha I(u) + \int_{-\infty}^{\infty}\left(\frac{\beta}{6}u^3 - \frac{1}{2}\gamma u\mathrm{H}u + \frac{1}{2}\delta u_x^2\right)dx, \tag{4}
\end{align}
$$

are preserved by sufficiently smooth, suitably vanishing at infinity solutions of (1). The quantity (4) determines the Hamiltonian formulation of (1)

$$u_t = J\delta E(u), \quad J = -\partial_x.$$

in suitable function spaces and where $\delta E$ denotes the variational derivative.

Solitary-wave solutions $u(x,t) = \varphi(x - c_s t), c_s > 0$ of (1) were initially studied, in terms of existence, stability and asymptotic behaviour, by Benjamin in [4, 5, 6]. The profile $\varphi$ satisfies, assuming that $\varphi \to 0$ as $|x| \to \infty$, the equation

$$F(\varphi, \gamma) = \delta E(\varphi) - c_s\delta I(\varphi) = (-c_s + \alpha)\varphi + \frac{\beta}{2}\varphi^2 - \gamma\mathrm{H}\varphi - \delta\varphi'' = 0. \tag{5}$$

Benjamin argued for an oscillating behaviour of the profiles in some parts of the spatial domain and for a monotonic decay at infinity as $1/|x|^2$. A complete theory of existence and stability of solitary-wave solutions for small values of $\gamma$ is provided in [2].

Explicit formulas for the profiles (except in the KdV and BO cases) are not known. Several techniques of numerical approximation involve numerical continuation algorithms on some parameter in (1). Numerical continuation is applied in [2] to design a code to approximate the solitary waves. The results reveal some properties, such as the symmetry about their crests and (except in the KdV and BO cases) the existence of a finite number of oscillations. In addition, numerical studies in [19] suggest an inelastic interaction of solitary waves and consequently a nonintegrable character of (1) when $\gamma > 0, \delta > 0$.

Note that if we look for solutions of (5) in the form

$$\varphi(X) = -\frac{2(\alpha - c_s)}{\beta} \psi\left(\sqrt{\frac{\alpha - c_s}{\delta}} X\right), \qquad (6)$$

then the profile $\psi$ satisfies

$$Q(\psi, \tilde{\gamma}) = \psi - 2\tilde{\gamma}\mathrm{H}\psi - \psi'' - \psi^2 = 0, \qquad (7)$$

where

$$\tilde{\gamma} = \frac{\gamma}{2\sqrt{\delta(\alpha - c_s)}}. \qquad (8)$$

This is the notation used in [2]. When $\gamma$ (and therefore $\tilde{\gamma}$) is zero, we obtain the well known solitary-wave solutions of the KdV equation. Thus, we will consider (5) as dependent on $\gamma$ as a continuation parameter. The form (7) will be used when necessary.

The literature on the numerical computation of travelling-wave solution profiles of nonlinear wave equations includes many different techniques. Some variational methods [3, 12] are based on the minimization of some relevant functional; there are also classical procedures, such as shooting methods [33], fixed point iterations with stabilizing factors or renormalization methods [26, 25, 1], Newton-like methods [8, 10, 29, 30]. The so-called imaginary-time evolution methods (see [31] and references therein) are based on integrating numerically a related evolution equation, for which the profile is a stationary solution and in which $t$ is replaced by $it$. The squared-operator methods [32, 30] iterate a modified equation whose linearization operator at the profile is the square of that of the original equation, guaranteeing the convergence. Finally, 'iterative cleaning' procedures [7, 19, 13] generate a solitary-wave profile by running a time-stepping code with some initial condition, isolating the leading pulse and using it as a new initial condition for the code in an iterative way, taking advantage of the resolution of solutions into solitary waves.

In this paper we focus on continuation techniques and we apply them to the Benjamin equation. Section 2 describes two directions that the numerical continuation algorithm can follow. One is continuation by differentiation, assuming a smooth dependence of the solitary wave on the continuation parameter. This leads to the so-called Davidenko equation [27, 9]. A second way, which will be considered in this paper, is given by incremental methods. Here, the parameter interval is partitioned, and starting from a value of the continuation parameter for which the solitary-wave profile is known, we compute an approximation to the profile at the next value of the parameter. The iterative process can be implemented with many alternatives, some of which will be described and applied to the Benjamin equation. For each method, we will explain the theoretical formulation and its implementation in Section 3. The latter includes the choice of the spatial discretization. (In sections 2 and 3, the description of the methods is independent of the discretization used). As the classical treatment

of the nonlocal term makes use of the Discrete Fourier Transform (DFT), the pseudospectral discretization will be emphasized and used in Section 4. The study in sections 2 and 3 will be illustrated here with some numerical experiments of comparison between the methods. The numerical examples will be mainly focused on three aspects: the computational efficiency of the techniques, how they cooperate with the continuation algorithm, and the behaviour of the resulting solitary-wave profiles when used as initial data in a time-stepping code for the Benjamin equation. The generation of multipulse solitary waves of the Benjamin equation will also be treated.

## 2. Continuation algorithms

From now on we assume that (5) is discretized, in some way, on a sufficiently long interval $(-l, l)$ with periodic boundary conditions, giving rise to a system of equations

$$
\begin{aligned}
F_k(\varphi_h, \gamma) \quad \equiv \quad & (-c_s + \alpha)\varphi_{h,k} + \frac{\beta}{2} \left(G_h(\varphi_h)\right)_k \\
& -\gamma \left(\mathrm{H}_h \varphi_h\right)_k - \delta \left(D_h^2 \varphi_h\right)_k = 0, \quad k = 0, \ldots, N-1. \quad (9)
\end{aligned}
$$

In (9):

- $\varphi_h = (\varphi_{h,0}, \ldots, \varphi_{h,N-1})$ denotes the approximation to the values of $\varphi$ at the grid $x_j = -l + hj, j = 0, \ldots, N-1$, where $h = 2l/N$. It is assumed that $N$ is even and $\varphi_h$ is extended as a periodic function $\varphi_h = \{\varphi_j\}_{j \in \mathbb{Z}}, \varphi_{j+N} = \varphi_j$, defined on the extended uniform grid $x_j = -l + hj, j \in \mathbb{Z}$

- $G_h(\varphi)$ is an approximation of the nonlinear term $\varphi^2$.

- $\mathrm{H}_h$ and $D_h^2$ are, respectively, discretizations of the operators H and $\partial_{xx}$.

*2.1. Continuation by differentiation*

If we are interested in the computation of the profile $\varphi(\gamma^*)$, corresponding to some parameter value $\gamma^*$, a first way to implement the continuation procedure is by differentiation, [27]. By [2], there is an analytic mapping

$$
\begin{aligned}
\varphi : \Gamma &\to H^1(\mathbb{R}) \cap C^\infty(\mathbb{R}) \\
\gamma &\longmapsto \varphi(\gamma),
\end{aligned}
$$

satisfying (5) on some interval $\Gamma = [0, \gamma^*]$. If $\gamma_0 = 0$ $\varphi_0 = \varphi(\gamma_0)$ corresponds to the known KdV profile, and $\varphi = \varphi(\gamma)$ is a solution of the initial-value problem (ivp)

$$
\begin{aligned}
F'(\varphi, \gamma)\frac{d\varphi}{d\gamma} &= -\frac{\partial F}{\partial \gamma}(\varphi, \gamma), \quad \gamma \in (0, \gamma^*), \quad (10) \\
\varphi(0) &= \varphi_0,
\end{aligned}
$$

4

where $F'$ is the Frechet derivative with respect to $\varphi$. The system (10) is sometimes called the Davidenko equation [27, 9]. Then, an ODE solver on the interval $[0, \gamma^*)$ can be used to approximate the discrete version of (10):

$$
\begin{aligned}
F_h'(\varphi_h, \gamma) \frac{d\varphi_h}{d\gamma} &= -\frac{\partial F_h}{\partial \gamma}(\varphi_h, \gamma), \quad \gamma \in (0, \gamma^*), \\
\varphi_h(0) &= \varphi_{0,h},
\end{aligned}
$$

where $F_h = (F_{h,0}, \ldots, F_{h,N-1})$ is defined in (9). The resolution requires the computation and handling of the Jacobian $F_h'(\varphi_h, \gamma)$; the difficulties in the implementation will be described later, when treating Newton's method.

*2.2. Incremental methods*

In the present paper we will consider a second type of continuation technique that consists of defining an homotopic path

$$
\gamma_0 = 0 < \gamma_1 < \ldots < \gamma_M = \gamma^*,
$$

with some diameter $h_M = \gamma^*/M$ for some $M$ and intermediate values $\gamma_m = mh_M, m = 0, \ldots, M$. The idea is, to start from the known profile $\varphi_0 = \varphi(\gamma_0)$, and compute $\varphi(\gamma_m)$ from $\varphi(\gamma_{m-1})$ using an iterative method in (5) or the spatially discretized version (9) with $\varphi(\gamma_{m-1})$ (or an extrapolation from previous values) as the starting iteration. This class of techniques is known as 'incremental methods' . The literature considers many possibilities in the choice of the iteration procedure. In the case of the Benjamin equation and among the possibilities cited in the Introduction, we focused on several examples of two groups of methods: Variants of classical techniques such as fixed-point iteration or Newton's method, and squared-operator methods, based on considering a related equation and properties of the corresponding linearized operator, [30].

## 3. Description of some incremental methods and their application to the Benjamin equation

*3.1. Petviashvili method*

Several methods are modifications of the classical fixed-point procedure (which typically diverges for this kind of problems [25]). One of them is the Petviashvili method [26]. This was originally implemented to compute solitary waves of the ivp for the KPI equation; its use to compute stationary and solitary-wave solutions has also been proposed in many places (see [25, 20] and references therein). The method is a version of the fixed-point iteration with a suitable iteration function. The equations (9) can be written as the system

$$
S_h \varphi_h \equiv \left( -c_s + \alpha - \gamma \mathrm{H}_h - \delta D_h^2 \right) \varphi_h = -\frac{\beta}{2} \left( G_h \varphi_h \right).
$$

If the operator $S_h = (-c_s + \alpha) - \gamma \mathrm{H}_h - \delta D_h^2$ is invertible, then the approximate solitary wave $\varphi_h$ satisfies

$$\varphi_h = -\frac{\beta}{2} S_h^{-1} \left( G_h \varphi_h \right). \tag{11}$$

This corresponds to the equation satisfied by the exact profile $\varphi$

$$S\varphi = \left( (-c_s + \alpha) - \gamma \mathrm{H} - \delta \partial_{xx} \right) \varphi = -\frac{\beta}{2} \varphi^2. \tag{12}$$

The Fourier transform allows to write (12) in the form

$$\widehat{\varphi}(\xi) = -\frac{\beta}{2} \frac{\widehat{[\varphi^2]}(\xi)}{-c_s + \alpha - \gamma |\xi| + \delta \xi^2}.$$

The Petviashvili method incorporates a stabilizing factor to ensure convergence in the following way. If we multiply (12) by $\varphi$ and integrate, we obtain by the Parseval identity

$$
\begin{aligned}
m(\varphi) &= \frac{\int_{-\infty}^{\infty} \left( (-c_s + \alpha - \gamma \mathrm{H} - \delta \partial_{xx}) \varphi \right) \varphi dx}{\int_{-\infty}^{\infty} -\frac{\beta}{2} \varphi^2 \varphi dx} \\
&= \frac{\int_{-\infty}^{\infty} \left( -c_s + \alpha - \gamma |\xi| + \delta \xi^2 \right) |\widehat{\varphi}(\xi)|^2 d\xi}{\int_{-\infty}^{\infty} -\frac{\beta}{2} \widehat{[\varphi^2]}(\xi) \overline{\widehat{\varphi}(\xi)} d\xi} = 1.
\end{aligned}
$$

This suggests considering the stabilizing factor for the approximation and to formulate the Petviashvili method as the iteration procedure for (11)

$$\varphi_h^{[\nu+1]} = m_\nu^\epsilon \left( -\frac{\beta}{2} S_h^{-1} \left( G_h \varphi_h^{[\nu]} \right) \right), \nu = 0, 1, \ldots \tag{13}$$

for initial $\varphi_h^{[0]}$, $m_\nu = m \left( \varphi_h^{[\nu]} \right)$ and where the power $\epsilon$ is a free parameter that governs the iteration. In the case of convergence, it is expected that $m_\nu \to 1$ as $\nu \to \infty$. This convergence can be analyzed by using the theory explained in [25] (see also [20]). The results there, applied to our case, imply that if

$$\min_{x \in \mathbb{R}} |\psi(x)| < 1/2,$$

where $\psi$ is given in (6), then the method is locally convergent for $\epsilon \in (1, 3)$, with the maximum rate of convergence attained when $\epsilon = 2$. In addition, a technique to improve the rate of convergence of the Petviashvili method (and, in fact, of any iterative method to find solitary waves) is described in [20, 21] and called the mode elimination technique. This generates the so-called accelerated Petviashvili method.

*Pseudospectral formulation.* If the discretization (9) makes use of the discrete Fourier coefficients of $\varphi_h$, then (13) has the form

$$\left(\widehat{\varphi_h^{[\nu+1]}}\right)_p = \widetilde{m}_p^\epsilon \left(-\frac{\beta}{2}\right) \frac{\left(\widehat{G_h \varphi_h^{[\nu]}}\right)_p}{\left(-c_s + \alpha - \gamma \widehat{H_h}(p) + \delta \left(\widehat{D_h^2}(p)\right)\right)} \qquad (14)$$

$$p \in \mathbb{Z},$$

where $\left(\widehat{\varphi_h}\right)_p$ denotes the $p$−th discrete Fourier coefficient of $\varphi_h$, the stabilizing factor is approximated by using

$$\widetilde{m}_p = -\frac{\sum_{p \in \mathbb{Z}} \left(-c_s + \alpha - \gamma \widehat{H_h}(p) + \delta \left(\widehat{D_h^2}(p)\right)\right) | \left(\widehat{\varphi_h^{[\nu]}}\right)_p |^2}{\sum_{p \in \mathbb{Z}} \frac{\beta}{2} \left(\widehat{G_h \varphi_h^{[\nu]}}\right)_p \overline{\left(\widehat{\varphi_h^{[\nu]}}\right)_p}},$$

and $\widehat{H_h}(p), \widehat{D_h^2}(p)$ denote, respectively, the Fourier symbol of the approximations $H_h$ and $D_h^2$. In the case of the pseudospectral discretization, which will be used in this paper for the experiments, (14) is formulated as

$$\left(\widehat{\varphi_h^{[\nu+1]}}\right)_p = -\frac{\beta}{2} \widetilde{\widetilde{m}}_p^\epsilon \frac{\left(\widehat{\varphi_h^{[\nu]}. * \varphi_h^{[\nu]}}\right)_p}{(-c_s + \alpha - \gamma |p| + \delta p^2)},$$

$$-N/2 \leq p \leq N/2, \quad \nu = 0, 1, \ldots$$

where

1. The product $\varphi_h^{[\nu]}. * \varphi_h^{[\nu]}$ is understood componentwise.
2. The approximation to the stabilizing factor has the form

$$\widetilde{\widetilde{m}}_p = \frac{\sum''_{-N/2 \leq p \leq N/2} \left(-c_s + \alpha - \gamma |p| + \delta p^2\right) | \left(\widehat{\varphi_h^{[\nu]}}\right)_p |^2}{\sum''_{-N/2 \leq p \leq N/2} \frac{\beta}{2} \left(\widehat{\varphi_h^{[\nu]}. * \varphi_h^{[\nu]}}\right)_p \overline{\left(\widehat{\varphi_h^{[\nu]}}\right)_p}},$$

   (the double prime in the sums shows that the first and last terms are divided by two).
3. We took $D_h^2 = D^2$ (the square of the pseudospectral differentiation operator) and $H_h$ as the discretization of the operator H (with the periodic version of the Hilbert Transform) with discrete Fourier coefficient $\widehat{H_h \varphi}(p) = |p| \left(\widehat{\varphi}\right)_p$.

*3.2. SOM and MSOM methods*

Two other techniques to compute solitary-wave solutions of the Benjamin equation use a different point of view. One is the so-called SOM (Squared Operator Method) and its variant MSOM (Modified Squared Operator Method). A complete study of these algorithms and many references may be found in e. g. [32]. Consider the equation (12) written in the form

$$L_0\varphi \equiv -S\varphi - \frac{\beta}{2}\varphi^2 = 0$$

Let $M$ be a real-valued, positive definite Hermitian operator. Instead of integrating numerically the system

$$\varphi_t = \pm M^{-1}L_0\varphi,$$

to obtain approximations to the equilibrium $L_0\varphi = 0$, the idea consists of integrating

$$\varphi_t = -M^{-1}L^*M^{-1}L_0\varphi, \quad L = -S - \beta\varphi \tag{15}$$

where $L$ is the linearization operator of (12) at $\varphi$ and $*$ denotes the $L^2$ adjoint (in our case $L^* = L$). Use of the explicit Euler method leads to the iterative SOM

$$\varphi^{[\nu+1]} = \varphi^{[\nu]} - \left(M^{-1}LM^{-1}L_0\varphi\right)\Big|_{\varphi=\varphi^{[\nu]}}\Delta\tau. \tag{16}$$

The operator $M$ is introduced as a preconditioning operator, to accelerate the convergence. Typical choices of $M$ are the linear part of $L_0$ (when it is positive definite, or modified to be positive definite) and operators of the form $M = c - \partial_{xx}$ for some constant $c$. When $M = I$, the implementation is simpler but the convergence is very slow. The choice of the Euler method is justified in [32] with the argument that other time-stepping schemes require more computations, making the resulting iteration less efficient. This technique is related to the functional minimization method for Hamiltonian equations, proposed and explained in [15]; see the comments in [32].

The implementation of (16) requires splitting the second term on the right-hand side into four terms. Taking into account the form of $L_0$ and $L$, we have

$$\begin{aligned}
\varphi^{[\nu+1]} &= \varphi^{[\nu]} - \Delta\tau\left[M^{-1}SM^{-1}S\varphi^{[\nu]} + \frac{\beta}{2}M^{-1}SM^{-1}(\varphi_h^{[\nu]}.\ast\varphi_h^{[\nu]})\right.\\
&\quad \left. +\beta M^{-1}\varphi_h^{[\nu]}M^{-1}S\varphi_h^{[\nu]} + \frac{\beta^2}{2}M^{-1}\varphi_h^{[\nu]}M^{-1}(\varphi_h^{[\nu]}.\ast\varphi_h^{[\nu]})\right].
\end{aligned}$$

For the pseudospectral version used in the numerical experiments we took $M = c - \partial_{xx}$ and the last two terms in the expression in brackets above were computed with the suitable combination of FFT/IFFT.

The local convergence of (16) is ensured as long as $\Delta\tau$ is below a certain threshold. Explicitly, this happens when $\Delta\tau < \Delta\tau_{max}$, with $\Delta\tau_{max} =$

$-\frac{2}{\Lambda_{min}}$, where $\Lambda_{min}$ is the minimum eigenvalue of the squared operator $\mathcal{L} = -M^{-1}L^*M^{-1}L$. The selection of $\Delta\tau$ to optimize the convergence rate is made by minimizing the convergence factor

$$R = \max_{\Lambda} |1 + \Lambda\Delta\tau| = \max\{|1 + \Lambda_{max}\Delta\tau|, |1 + \Lambda_{min}\Delta\tau|\}, \tag{17}$$

for the nonzero eigenvalues $\Lambda$ of $\mathcal{L}$. The smallest $R$ occurs when, [32]

$$\Delta\tau = \Delta\tau_* = -\frac{2}{\Lambda_{max} + \Lambda_{min}}, \tag{18}$$

for which

$$R_* = \frac{\Lambda_{min} - \Lambda_{max}}{\Lambda_{min} + \Lambda_{max}}. \tag{19}$$

The Modified Squared Operator Method MSOM is a variant of the SOM whose goal is to identify and eliminate the most harmful direction that slows down the convergence. Its description and analysis are also made in [32] and the formulas for the MSOM are

$$\begin{aligned} \varphi^{[\nu+1]} &= \varphi^{[\nu]} - \left( M^{-1}LM^{-1}L_0\varphi \right. \\ &\quad \left. -\alpha^{[\nu]}\langle G^{[\nu]}, L^*M^{-1}L_0\varphi\rangle G^{[\nu]} \right)\Big|_{\varphi=\varphi^{[\nu]}}\Delta\tau. \end{aligned} \tag{20}$$

where

$$\alpha^{[\nu]} = \frac{1}{\langle MG^{[\nu]}, G^{[\nu]}\rangle} - \frac{1}{\Delta\tau\langle LG^{[\nu]}, M^{-1}LG^{[\nu]}\rangle},$$

and $G^{[\nu]} = \varphi^{[\nu]}$ or $G^{[\nu]} = \varphi^{[\nu]} - \varphi^{[\nu-1]}$. Local convergence of (20) is ensured under the conditions for the convergence of the SOM, plus the assumptions $LG^{[0]} \neq 0$ and

$$\Delta\tau < \Delta\tau_M = \min\left(-\frac{2}{\Lambda_{min}}, \frac{1}{\beta - \Lambda_{min}}\right), \quad \beta = \frac{\langle MG^{[0]}, \mathcal{L}G^{[0]}\rangle}{\langle MG^{[0]}, G^{[0]}\rangle}.$$

The appendix in [32] provides a family of more general squared operator methods, by introducing powers of the acceleration operator $M$. Compared to (16), the implementation of (20) has the extra cost of computing the second term in the parenthesis. In all cases, and for the pseudospectral approximation used in this paper, the inner products have been computed via the Parseval identity, the second choice of $G^{[\nu]}$ has been used and $M = c - \partial_{xx}$. The latter gave slightly better results (with suitable values of $c$) than other alternatives, as, for example, the linear part of $L_0$.

*3.3. CG-Newton method*

The last technique described in this report is the so-called Conjugate Gradient Newton method, or CGN method, [29]. Given $\varphi^{[\nu]}$, Newton's method

9

generates the next iterate with the formulas

$$\varphi^{[\nu+1]} = \varphi^{[\nu]} + \Delta\varphi^{[\nu]}, \tag{21}$$

$$L_\nu \Delta\varphi^{[\nu]} = -L_0\varphi^{[\nu]}, \tag{22}$$

where $L_\nu$ is the linearization operator in (15) evaluated at $\varphi^{[\nu]}$. The classical Newton's method uses direct methods to solve (22). Its implementation, for the computation of travelling-wave profiles, is usually affected by several difficulties, mainly due to the singular Jacobian operator, the translational invariance of the equation under study, and the possibility of small denominators, [2, 10, 11]. In particular, since (1) is invariant under spatial translations, the approximations to $L_\nu$ will be singular or almost singular and the previously mentioned computational problems will be present in this case. This can be avoided by imposing the symmetry of the profile at $x = 0$, [10]. In the case of spectral methods, this symmetry condition can be imposed by using only cosine bases, instead of the complex exponential, and omitting the constant, [9]. To this end, one of the Discrete Cosine Transforms (DCT) and its fast version may be used. In the case of (1), the implementation of the DCT is not trivial, since it must take into account the treatment, in the frequency domain, of the differential and nonlocal operators, along with the convolution, [24, 23, 28]. Furthermore, an additional problem is present, [8], since, due to the convolution and the nonlocal terms, the whole computation of $L_\nu$ is required.

An alternative to the classical version is given by the resolution of the discrete version of (22) with the Conjugate Gradient method, [16], using the fact that $L$ is self-adjoint. The iteration is usually preconditioned by a self-adjoint and positive definite acceleration operator $M$. Note that in the case of the Benjamin equation the technique must consist then of three processes: the homotopy procedure, the advance of the approximation (21), and the (preconditioned) Conjugate Gradient iteration to obtain the incremental term $\Delta\varphi^{[\nu]}$. Taking $\Delta\varphi^{(0)} = 0$ for simplicity, the Preconditioned Conjugate Gradient method for the Newton correction (22) has, in its $i$-th iteration, the following form, [29]:

$$
\begin{aligned}
R^{(0)} &= -L_0\varphi^{[\nu]}; D^{(0)} = M^{-1}R^{(0)}, \\
a^{(i)} &= \frac{\langle R^{(i)}, M^{-1}R^{(i)} \rangle}{\langle D^{(i)}, L_\nu D^{(i)} \rangle}, \\
\Delta\varphi^{(i+1)} &= \Delta\varphi^{(i)} + a^{(i)}D^{(i)}, \\
R^{(i+1)} &= R^{(i)} - a^{(i)}L_\nu D^{(i)}, \\
b^{(i+1)} &= \frac{\langle R^{(i+1)}, M^{-1}R^{(i+1)} \rangle}{\langle R^{(i)}, M^{-1}R^{(i)} \rangle}, \\
D^{(i+1)} &= M^{-1}R^{(i+1)} + b^{(i+1)}D^{(i)}.
\end{aligned}
\tag{23}
$$

The standard $L^2$ inner product is used. It is worth recalling some remarks from [29]. Normally, the Conjugate Gradient method may be applied to self-adjoint, positive definite operators. When this is not satisfied, an alternative version of (23) can be used, [29, 30]. On the other hand, the zero eigenvalue of $L$, which

makes the solution of (22) not unique and generates the previously mentioned computational problems in Newton's method, does not seem to cause a trouble here. The symmetry of the profile is ensured in a simple way, [29], by taking an even initial guess $\varphi^{[0]}$. As mentioned before, a resolution with direct methods also has the same problem (the discretization of $L$ is usually a singular, or nearly singular, matrix) and it can be corrected similarly, but the imposition of this assumption is computationally harder, [10].

For the corresponding pseudospectral version of the method used in the next section, all computations are performed in the Fourier space and have, in the $i$th inner iteration, the form

$$\left(\widehat{R^{(0)}}\right)_p = \left(-c_s + \alpha - \gamma|p| + \delta p^2\right)\left(\widehat{\varphi_h^{[\nu]}}\right)_p + \frac{\beta}{2}\left(\widehat{\varphi_h^{[\nu]}.* \varphi_h^{[\nu]}}\right)_p,$$

$$\left(\widehat{D^{(0)}}\right)_p = \frac{\left(\widehat{R^{(0)}}\right)_p}{c + p^2},$$

$$\left(\widehat{LD^{(i)}}\right)_p = \left(-c_s + \alpha - \gamma|p| + \delta p^2\right)\left(\widehat{D^{(i)}}\right)_p + \beta\left(\widehat{\varphi_h^{[\nu]}D^{(i)}}\right)_p,$$

$$a^{(i)} = \frac{\sum''_{-N/2 \le p \le N/2}|\left(\widehat{R^{(i)}}\right)_p|^2/(c+p^2)}{\sum''_{-N/2 \le p \le N/2}\left(\widehat{LD^{(i)}}\right)_p\overline{\left(\widehat{D^{(i)}}\right)_p}},$$

$$\left(\widehat{\Delta\varphi^{(i+1)}}\right)_p = \left(\widehat{\Delta\varphi^{(i)}}\right)_p + a^{(i)}\overline{\left(\widehat{D^{(i)}}\right)_p},$$

$$\left(\widehat{(R^{(i+1)}}\right)_p = \left(\widehat{(R^{(i)}}\right)_p - a^{(i)}\left(\widehat{LD^{(i)}}\right)_p,$$

$$b^{(i+1)} = \frac{\sum''_{-N/2 \le p \le N/2}|\left(\widehat{R^{(i+1)}}\right)_p|^2/(c+p^2)}{\sum''_{-N/2 \le p \le N/2}|\left(\widehat{R^{(i)}}\right)_p|^2/(c+p^2)},$$

$$\left(\widehat{D^{(i+1)}}\right)_p = \frac{\left(\widehat{R^{(i+1)}}\right)_p}{c+p^2} + b^{(i+1)}\widehat{\left(D^{(i)}\right)}_p.$$

## 4. Numerical experiments

### 4.1. Introductory remarks and parameter selection for the methods

In this section we present a series of numerical experiments to compare these methods for the generation of solitary-wave profiles for the Benjamin equation (1), (9). The values $\alpha = 1, \beta = 1, \delta = 1, c_s = 0.75$ have been fixed, so that the continuation parameter is $\gamma$. Following [2], waves of physical relevance correspond to $\gamma$ between 0 and 1. (Note that with the previous values, $\gamma$ coincides with the $\tilde{\gamma}$ in (8)). The techniques implemented will be: the Petviashvili method [PM], the SOM ([SOM]) and MSOM ([MSOM]) methods, and the Conjugate-Gradient Newton method ([CGN]). The homotopy algorithm has

been performed with a stepsize $\Delta\gamma = 10^{-3}$. The solitary-wave profile is then computed at values $\gamma_j = \gamma_0 + j\Delta\gamma, j = 1, \ldots, M$, with $\gamma_0 = 0$, for which the solitary wave is known (KdV). The performance of each method will be analyzed at the final value of the $\gamma$ considered and at a general step of the numerical continuation, from $\gamma_j$ to $\gamma_{j+1}$.

The error at the $\nu$-th step of the iteration has been measured by

$$E^{[\nu]} = \frac{||\varphi_h^{[\nu]} - \varphi_h^{[\nu-1]}||}{||\varphi_h^{[\nu]}||},$$

in the Euclidean norm. For the [CGN], the norm of the residual error

$$EL^{[\nu]} = ||L_0 \varphi_h^{[\nu]}||, \tag{24}$$

has also been used. Three parameters control the procedure: The iteration stops when a maximum number of iterations is exceeded, or when the errors $E^{[\nu]}$ or $EL^{[\nu]}$ are smaller than a given tolerance $TOL$. This general strategy has some variants, depending on the specific implementation of the method, especially in the value of $TOL$ and the way of counting the number of iterations.

The numerical experiments can be divided into two groups. The first makes general comparisons between the methods by measuring the errors as functions of the number of iterations and of the cpu time. The second group uses the results of the most efficient method, to emerge the first group of experiments. The corresponding profiles are taken as initial conditions of a numerical evolution method integrating (1) in time. The evolution of the approximate solitary waves is monitored up to $T = 300$. The goal here is to study the accuracy of the computed profiles.

The study of comparison of the methods requires first some preliminary remarks concerning particular aspects of each of them. For the [PM], the local convergence can be observed by studying the stabilizing factor $m_\nu$ in one continuation step $\gamma_j \mapsto \gamma_{j+1}$, Figure 1 shows, for the values of $\gamma$ indicated, the behaviour of the error in the stabilizing factor $M$ as a function of the number of iterations. When $\gamma > 0.1$, similar results are observed. It is also noted that the stabilizing factor approaches 1 to machine accuracy quite fast. For instance, for $\gamma = 0.034$, the discrepancy $|m_\nu - 1|$ is $O(10^{-13})$ in $NITER = 15$ iterations and $O(10^{-16})$ when $NITER = 25$.

For the [SOM] and [MSOM], the corresponding discrete version of $M = c - \partial_{xx}$ has been taken as the preconditioning operator. The behaviour of these two methods strongly depends on the parameters $c, \Delta\tau$ and $\gamma$. The main conclusion is that as $\gamma \uparrow 1$, the rate of convergence of the methods goes to one very fast. This slows down both and sometimes prevents the SOM and MSOM to be competitive to other alternatives, specially for $\gamma$ close to 1.

The techniques described in [32] to estimate the rate of convergence of the SOM can be applied in the case at hand. They are as follows: For some values of $c$, the eigenvalues of the discretization of the iteration operator $\mathcal{L}$ are computed. Then the convergence factor $R_*(c)$ is calculated from (19). The dependence of
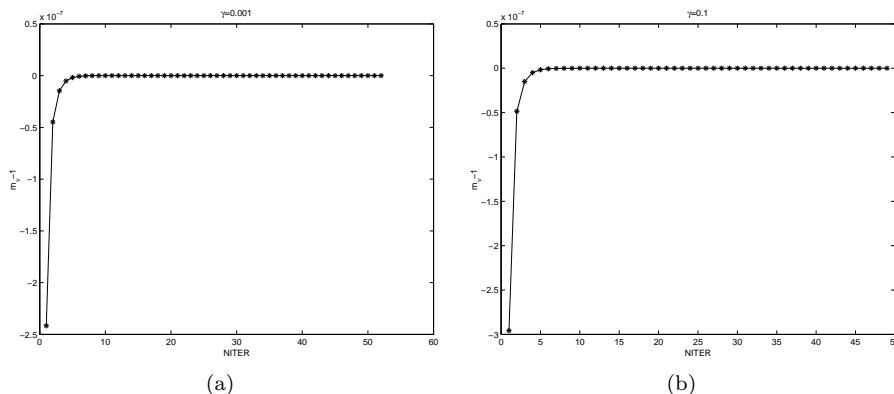
Figure 1: Discrepancy $m_\nu - 1$ of the stabilizing factor of [PM] vs. number of iterations for the continuation steps: (a) $0 \mapsto 0.001$; (b) $0.099 \mapsto 0.1$.

| $\gamma$ | $c_{opt}$ | $R_*(c_{opt})$ | $\Delta\tau_{opt}$ |
|---|---|---|---|
| 0.1 | 0.248 | 0.203 | 1.0641 |
| 0.5 | 0.259 | 0.602 | 1.653 |
| 0.9 | 0.270 | 0.979 | 2.274 |
| 0.95 | 0.270 | 0.995 | 2.310 |
| 0.99 | 0.270 | 0.999 | 2.326 |

Table 1: [SOM]: Computed values of $c_{opt}, R_*(c_{opt})$ and $\Delta\tau_{opt}$.

$R_*$ on $\Delta\tau$ is obtained by estimating (17) for some values of the step size. The optimal $\Delta_{opt}\tau$ practically coincides with that of formula (18).

For the solitary-wave profile it is necessary to compute the iteration matrix, (see the operator $\mathcal{L}$ in (15)). In the following experiments, for each value of $\gamma$, we compute the solitary wave given by the [PM] with $N = 512$ points on the interval $[-64, 64]$.

Figure 2 shows, for $\gamma = 0.1, 0.5, 0.9, 0.99$, the convergence rate $R_*(c)$ as a function of $c$. Its minimum value, and the corresponding value of $c = c_{opt}$ are shown in Table 1. Observe that, as $\gamma$ tends to 1, the minimum of $R_*$ also grows, becoming, for the last $\gamma$, very close to one.

Figure 3 shows the rate $R$, evaluated at the optimal $c = c_{opt}$, as a function of $\Delta\tau$. The value of the step size which gives the minimum, $\Delta\tau_{opt}$, coincides with the value given by (18) to four digits, since $\Delta\tau = 10^{-3}$.

These experiments do not seem to recommend choosing [SOM], at least for $\gamma$ close to one. Observe that the dependence on $\gamma$ is also somehow incompatible with the continuation algorithm. For instance, the value of $\Delta\tau_{opt}$ corresponding to $\gamma = 0.9$ gives values of $R$ that are far from the corresponding minimum $R_*$ associated with previous values of $\gamma$. Hence, it is hard to establish a common $\Delta\tau_{opt}$ for the whole continuation algorithm. An alternative strategy would be

13
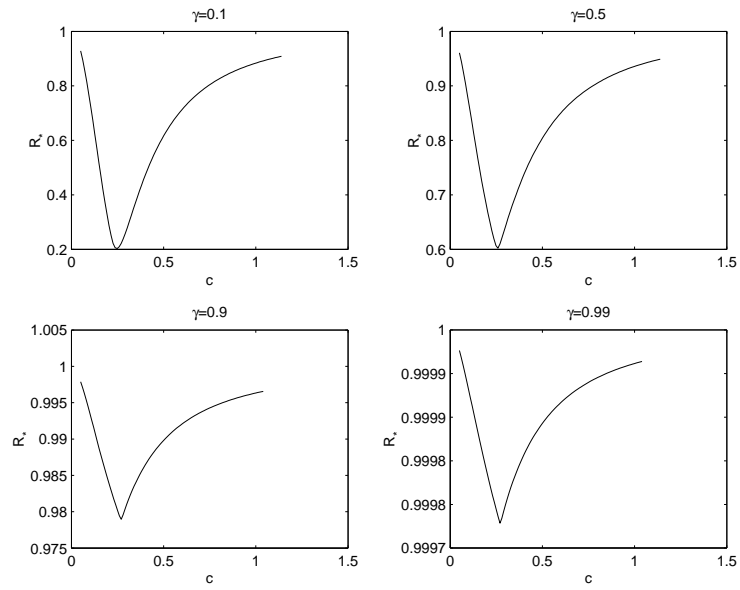
Figure 2: [SOM]: Convergence rate $R$ vs. $c$ following formula (19).
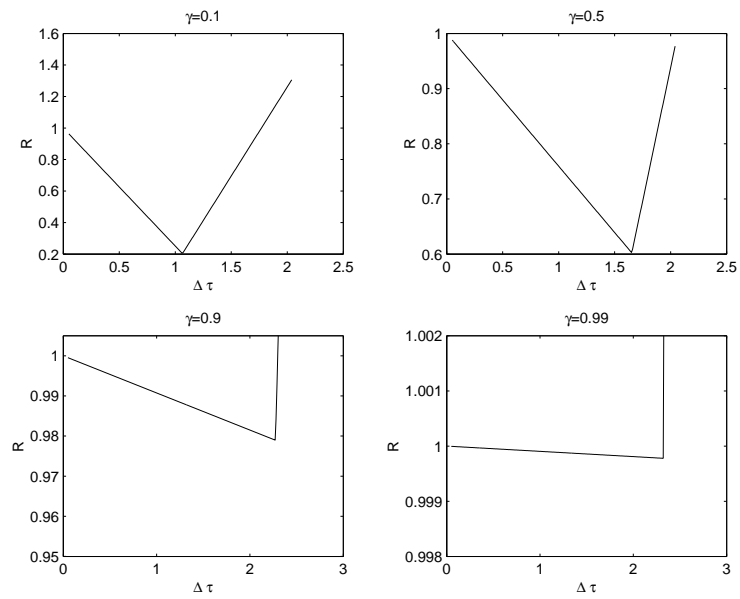


Figure 3: [SOM]: Convergence rate $R = R(\Delta\tau, c_{opt})$ vs $\Delta\tau$ following formula (17).

14

to compute the best value of $c$ and $\Delta\tau$ for each $\gamma$, but this is very costly.

The first points to emphasize in the case of [CGN] are the stopping criteria and the number of iterations. Recall that the method contains, in a step $\gamma_j \mapsto \gamma_{j+1}$, two loops, corresponding to the advance of the Newton correction and to the application of the CG method. For the first one, the stopping criterion is controlled by a fixed maximum number of iterations and by a small tolerance ($TOL = 10^{-15}$ in our case) for the residue $EL^{[\nu]}$. For the CG iteration, the technique described in [29] has been used. This adapts the process to the accuracy of the outer iteration. The error is measured by the norm of the function $R^{(i)}$ in the CG formulas, so that if

$$||R^{(i)}||_M < \epsilon_{CG}||R^{(0)}||_M,$$

the iteration stops. Here $||\cdot||_M$ is the $M^{-1}$-weighted $L^2$ norm

$$||\varphi||_M = \langle \varphi, M^{-1}\varphi \rangle^{1/2}, \quad M = c - \partial_{xx},$$

where $\langle \cdot, \cdot \rangle$ denotes the $L^2$ inner product in $(-l, l)$, $R^{(0)} = -L_0\varphi^{[\nu]}$ is the residue of the method and $\epsilon_{CG}$ is an error tolerance parameter, which relates the two iterations. In order to optimize the two procedures, it is recommended in [29] to take $\epsilon_{CG}$ between $10^{-1}$ and $10^{-3}$. We found that $\epsilon_{CG} = 10^{-2}$ gives good results in our case. Finally, the comparisons with other methods, shown in figures 9 and 10, are made by computing the error with the usual $L^2$ norm of the residue (24).

The implementation of two iterative procedures implies the existence of two iterations: one for the Newton correction and one for the CG method. The Newton correction requires one or two iterations, so we have chosen to present data for the total number of inner CG iterations. This number estimates the global computational cost of the method.

On the other hand, the [CGN] method also requires the selection of the parameter $c$ of the preconditioning operator. The data of Figure 4 may be used as an aid to this. The figure shows, for five values of $\gamma$, the number of iterations (left) and the CPU time (right) versus the parameter $c$. Figure 4 suggests that the best value of $c$ is likely to be in the interval $[0.25, 0.3]$. A further refinement suggests that $c = 0.275$ is a good value; this was used in the numerical experiments in the sequel.

### 4.2. A comparative study of generation of solitary waves

#### 4.2.1. Solitary-wave profiles

Figure 5 shows some solitary-wave profiles of the Benjamin equation obtained with the [PM] by using a pseudospectral code with $N = 2048$ points on the interval $[-256, 256]$, from the known KdV profile ($\gamma = 0$) to the one corresponding to $\gamma = 0.99$. The generation of the symmetric lobules (whose number increases with $\gamma$) is observed (cf. [2]). It is worth mentioning that the other methods gave entirely similar profiles. Some differences in their performance will be pointed out below.
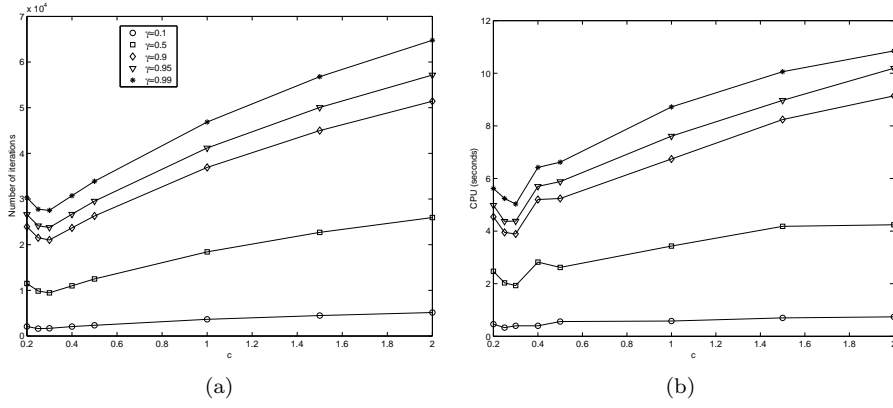
Figure 4: [CGN]: Number of iterations (a) and CPU time (b) vs. $c$.
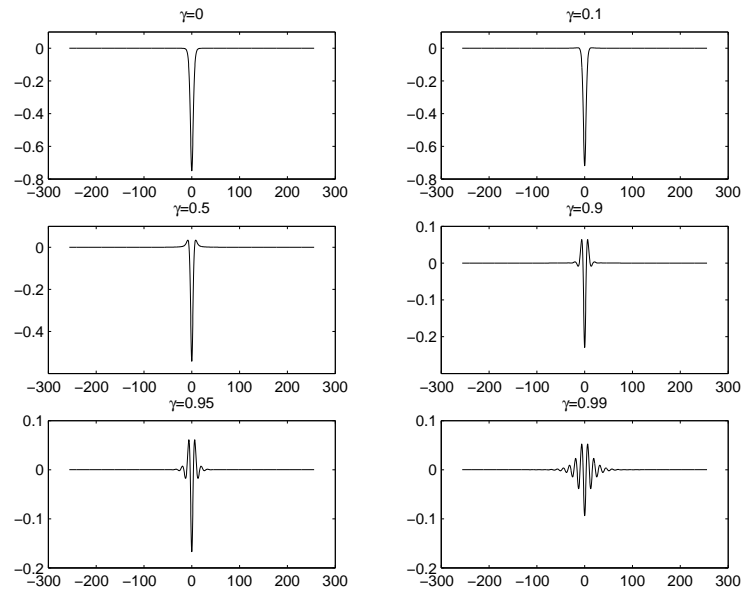


Figure 5: Solitary-wave profiles for the [PM] on the interval $[-256, 256]$ and with $N = 2048$.

16

| $\gamma$ | NITER | CPU (SEC) | NITER (MEAN VALUE) |
|---|---|---|---|
| 0.1 | 5040 | 2.03 | 50.4 |
| 0.5 | 22436 | 9.68 | 43.5 |
| 0.9 | 35374 | 15.25 | 32.4 |
| 0.95 | 38074 | 16.44 | 54.0 |
| 0.99 | 42517 | 18.47 | 111.1 |

Table 2: Number of iterations and CPU time for solitary-wave generation with the [PM].

| $\gamma$ | NITER | CPU (SEC) | NITER (MEAN VALUE) |
|---|---|---|---|
| 0.1 | 8410 | 7.64 | 84.1 |
| 0.5 | 51457 | 48.78 | 108.3 |

Table 3: Number of iterations and CPU time for solitary-wave generation with the [SOM]. The computations corresponding to $\gamma = 0.9$ attained the maximum ($10^5$) of iterations.

*4.2.2. Continuation procedure*

As noted before, the continuation method was implemented with a stepsize $\Delta\gamma = 10^{-3}$, while the tolerance for the procedures was taken as $TOL = 10^{-15}$ for all methods except for [SOM], where we took $TOL = 5 \times 10^{-15}$. Table 2 shows, for [PM], the total number of iterations and the cpu time required to get to the corresponding value of $\gamma$, when the errors in each iterative step, $E^{[\nu]}$ or $EL^{[\nu]}$, are less than the tolerance. The last column shows the mean number of iterations required in an application of the [PM]; that is, to go from $\gamma_j$ to the next one $\gamma_{j+1} = \gamma_j + \Delta\gamma$. These values are computed from information from the interval of the two most recent values of $\gamma$. (For example, the quantity 43.5 for $\gamma = 0.5$ is obtained by calculating the mean value of iterations between $\gamma = 0.1$ and $\gamma = 0.5$; the quantity 32.4 is obtained using the iterations between $\gamma = 0.5$ and $\gamma = 0.9$, and so on). This may help to identify the range of $\gamma$ for which the iterative process is slower. In this sense, it is seen that for the last values of $\gamma$ (when the oscillations grow in number), the computations seem to be harder. While up to $\gamma = 0.9$, the [PM] computes a step $\gamma_j \mapsto \gamma_{j+1}$ in not more than 50 iterations, this number starts to grow for $\gamma$ greater than 0.95 and, for instance, the method requires the same CPU time and number of iterations to go from $\gamma = 0$ to $\gamma = 0.1$ as those to go from $\gamma = 0.95$ to $\gamma = 0.99$. The global mean value of iterations, up to $\gamma = 0.99$, is about 42.95.

Table 3 provides the same information but for [SOM]. (Here the computation for $\gamma = 0.9$ attained the maximum number of iterations allowed). Clearly, the convergence is slow. The situation is slightly different in the case of [MSOM]. (Here we used the same values of $c$ and $\Delta\tau$ as in [SOM]). The improvement, compared to [SOM], can be seen in Table 4. (At $\gamma = 0.99$, the maximum number of iterations is attained and the results are not shown). We observe that, for a smaller tolerance ($TOL = 10^{-15}$ now), the [MSOM] is able to give results for

| $\gamma$ | NITER | CPU (SEC) | NITER (MEAN VALUE) |
|------|-------|-----------|--------------------|
| 0.1  | 3743  | 3.90      | 37.4               |
| 0.5  | 21546 | 22.54     | 44.5               |
| 0.9  | 58075 | 62.34     | 91.3               |
| 0.95 | 79328 | 85.84     | 531.3              |

Table 4: Number of iterations and CPU time for solitary-wave generation with the [MSOM] and $TOL = 10^{-15}$. The computations corresponding to $\gamma = 0.99$ attained the maximum $(10^5)$ of iterations.

| $\gamma$ | NITER | CPU (SEC) | NITER (MEAN VALUE) |
|------|-------|-----------|--------------------|
| 0.1  | 1577  | 0.29      | 15.8               |
| 0.5  | 9351  | 2.26      | 19.4               |
| 0.9  | 20842 | 4.29      | 28.7               |
| 0.95 | 23515 | 4.76      | 66.8               |
| 0.99 | 27185 | 5.32      | 91.8               |

Table 5: Number of iterations and CPU time for solitary-wave generation with the [CGN]. $TOL = 10^{-15}$.

$\gamma$ greater than 0.9 in a computationally reasonable time improving those of the [SOM].

In the case of the [CGN], with $\epsilon_{CG} = 10^{-2}, TOL = 10^{-15}, c = 0.275$, the corresponding information about the continuation process appears in Table 5. The best performance of the [CGN] is evident, specially for values of $\gamma$ closer to one. To verify this, in Figure 6, the number of iterations and the CPU time are displayed as functions of $\gamma$, for the three more competitive methods. The Petviashvili method [PM] continues to be more efficient in the global continuation procedure than [MSOM], both in number of iterations and computational time, although these are comparable for small values of $\gamma$.

*4.2.3. Iteration errors*

The four methods can also be compared in terms of the iteration errors. Figure 7 shows, for small values of $\gamma$, the logarithm of the error $E^{[\nu]}$ against the number of iterations needed by the [SOM], the [PM] and the [MSOM]. In all cases, the [MSOM] appears as the most efficient. However, this best performance of the [MSOM] does not continue as $\gamma$ grows. This is observed in Figure 8. Here, [MSOM] and [PM] are compared with values of $\gamma$ closer to one and [PM] behaves better.

The comparison of the errors associated with the residue reveals that [CGN] has the advantage. Figure 9 shows, for small values of $\gamma$, the $L^2$ norm of the error of the corresponding residue as a function of the number of iterations. This figure shows that the [CGN] attains, for a fixed number of iterations, the smallest error, and needs, for a fixed error level, the minimum number of

18
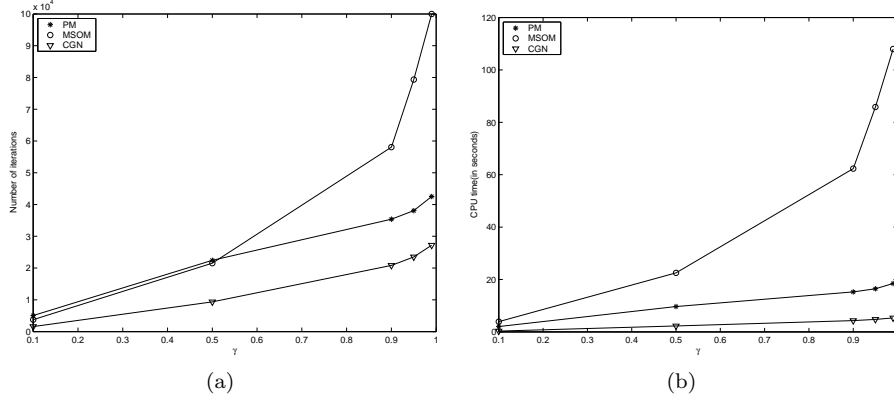
Figure 6: Number of iterations (a) and CPU time (b) vs. $\gamma$, for [PM], [MSOM] and [CGN].
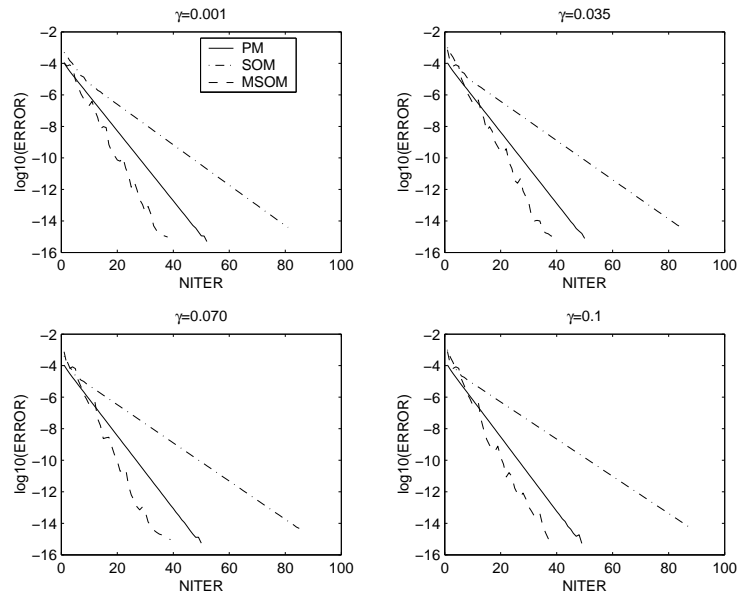


Figure 7: Logarithm of the error $E^{[\nu]}$ vs number of iterations for the continuation steps: $0 \mapsto 0.001, 0.034 \mapsto 0.035, 0.069 \mapsto 0.070, 0.099 \mapsto 0.1$.
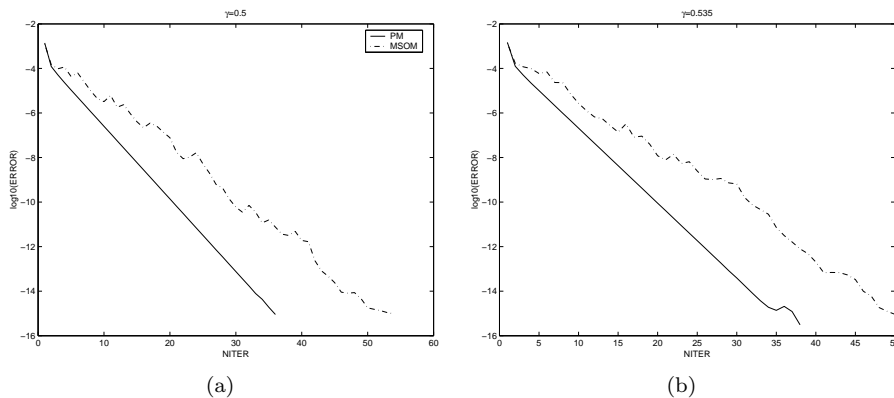
Figure 8: Logarithm of the error $E^{[\nu]}$ vs number of iterations for the continuation steps: (a) $0.499 \mapsto 0.5$; (b) $0.534 \mapsto 0.535$.

iterations. This persists during the whole continuation procedure, as it can be seen, for example, for some values of $\gamma$ close to 0.5 and the three methods [PM], [MSOM] and [CGN], in Figure 10.

### 4.3. Multi-pulse solitary waves

We used [CGN], the method that emerged as the most efficient from the single solitary-wave computations outlined above, to compute *multi-pulse solitary wave solutions* of the Benjamin equation. We started the continuation procedure at $\gamma = 0$ using as initial profile a linear superposition of KdV solitary waves of the same amplitude (corresponding to $c_s = 0.75$) and whose centers are located at $x = -10, 10$ (in the case of a two-pulse) and at $x = -10, 0, 10$ (in the case of a three-pulse). We used $N = 2048$ points on the interval $[-256, 256]$.

Figure 11 shows the profiles of two-pulse solitary waves that emerged from the [CGN] procedure for different values of $\gamma$, while three-pulses are captured in Figure 12. In these experiments, the performance of the numerical method deteriorated. For instance, we have observed that, in the case of two-pulses, and $\gamma = 0.99$ [CGN] was not convergent. Figure 13 displays a magnification of the three-pulses generated when $\gamma = 0.9, 0.95$.

### 4.4. Temporal evolution of numerical solitary waves

A necessary test to evaluate the accuracy of the computed solitary-wave profiles is checking that they are travelling-wave solutions of the time-dependent partial differential equation. To this end, we took the solitary-wave profiles generated by [CGN] as initial conditions and integrated the Benjamin equation in time, monitoring the amplitude and speed to assess the accuracy of the travelling-wave numerical solution. The numerical method here uses a pseudospectral discretization in space, while the temporal integration is carried out with the third-order SDIRK method, (see e. g. [18] and references therein), corresponding to the tableau

20
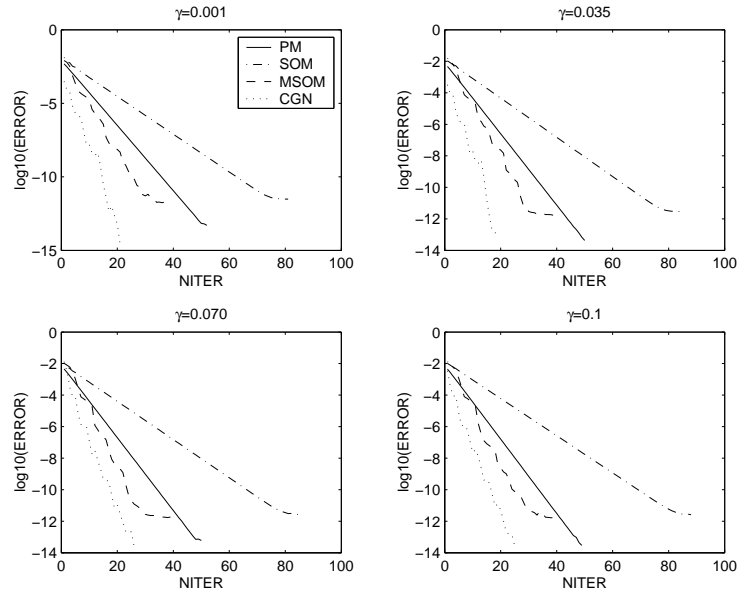
Figure 9: Logarithm of the error $EL^{[\nu]}$ vs number of iterations for the continuation steps: $0 \mapsto 0.001, 0.034 \mapsto 0.035, 0.069 \mapsto 0.070, 0.099 \mapsto 0.1$.
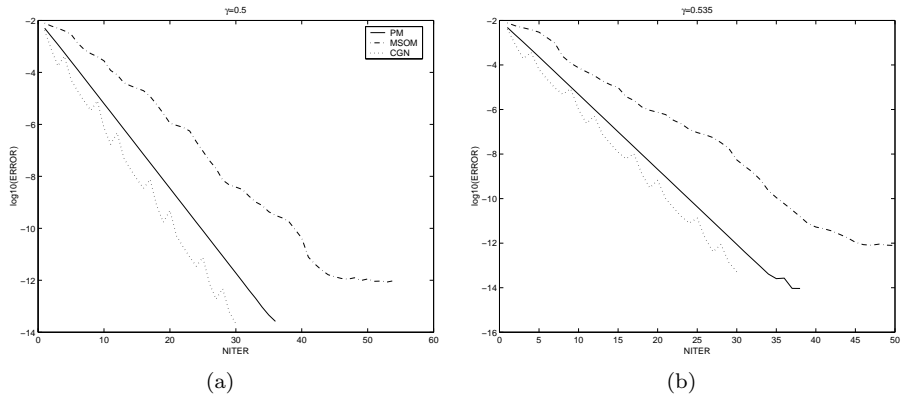


Figure 10: Logarithm of the error $EL^{[\nu]}$ vs number of iterations for the continuation steps: (a) $0.499 \mapsto 0.5$; (b) $0.534 \mapsto 0.535$.
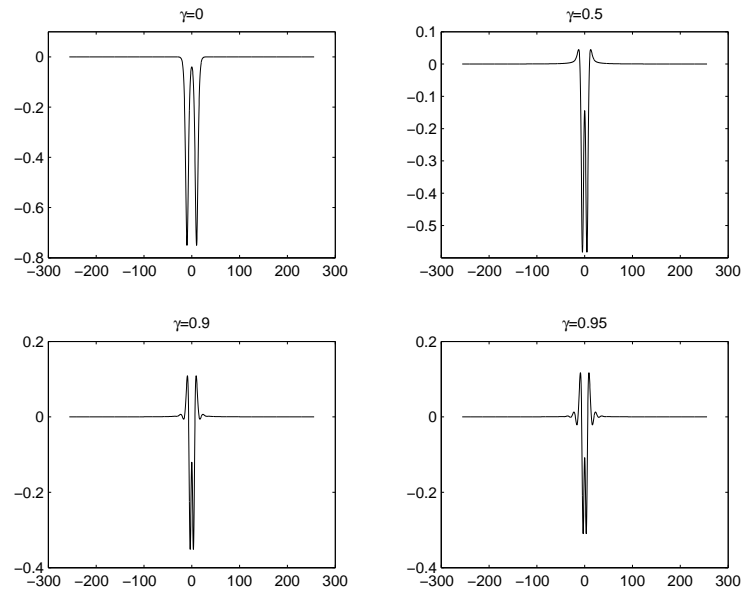
Figure 11: Two-pulse solitary-wave profiles for the [CGN] on the interval $[-256, 256]$ and with $N = 2048$.
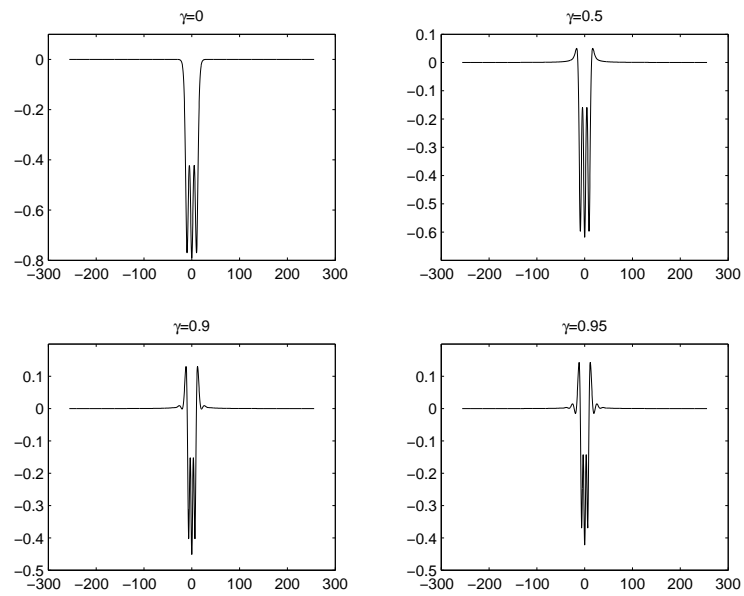


Figure 12: Three-pulse solitary-wave profiles for the [CGN] on the interval $[-256, 256]$ and with $N = 2048$.

22
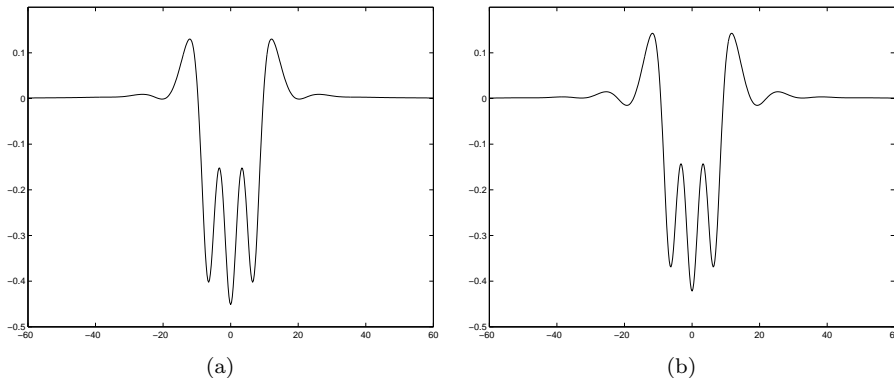
Figure 13: Three-pulse solitary-wave profiles for the [CGN] on the interval $[-256, 256]$ and with $N = 2048$. Magnification of Figure 12 for: (a) $\gamma = 0.9$; (b) $\gamma = 0.95$.

$$\begin{array}{c|cc} \frac{3+\sqrt{3}}{6} & \frac{3+\sqrt{3}}{6} & 0 \\ \frac{3-\sqrt{3}}{6} & \frac{-\sqrt{3}}{3} & \frac{3+\sqrt{3}}{6} \\ \hline & \frac{1}{2} & \frac{1}{2} \end{array}, \tag{25}$$

and modified with a projection technique, [17], to preserve the discrete versions of the invariants $C$ and $F$, in (2) and (3) respectively, defined as

$$C_h(Z) = h \sum_{j=0}^{N-1} Z_j, \quad I_h(Z) = \frac{h}{2} \sum_{j=0}^{N-1} Z_j^2,$$

for $Z = (Z_0, \ldots, Z_{N-1})^T$. We observe that preservation of the discrete version of the Hamiltonian (4), $E_h = \alpha I_h + G_h$ with

$$G_h(Z) = h \left( \sum_{j=0}^{N-1} \frac{\delta}{2} (DZ)_j^2 - \frac{\gamma}{2} (Z_j (H_h Z)_j) + \frac{\beta}{6} (Z)_j^3 \right),$$

cannot be simultaneously achieved. The reason is that at the exact solitary wave, the quantities $\delta E$ and $\delta I$ are dependent, as (5) shows. This also happens in the discrete case. Thus, the numerical projection technique to preserve the discrete versions of the functionals, applied to $E$ and $I$ at the same time, [17, 18], does not work.

The step sizes have been taken as $h = 0.25$ for the spatial pseudospectral discretization (used for the computation of the initial profiles as well) and $\Delta t = 6.25 \times 10^{-3}$ for the temporal discretization. (Smaller values of $\Delta t$ did not change the results significantly).

Figures 14, 15, and 16 show the evolution of the initial profile, corresponding to $\gamma = 0.5, 0.9, 0.99$ respectively, up to time $t = 300$. More information is

23

(a)          (b)          (c)
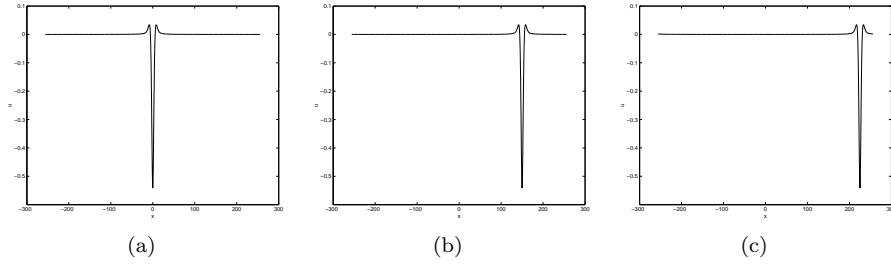
Figure 14: Numerical solution from the initial s-w profile for $\gamma = 0.5$: (a) $t = 0$; (b) $t = 200$; (c) $t = 300$.



(a)          (b)          (c)
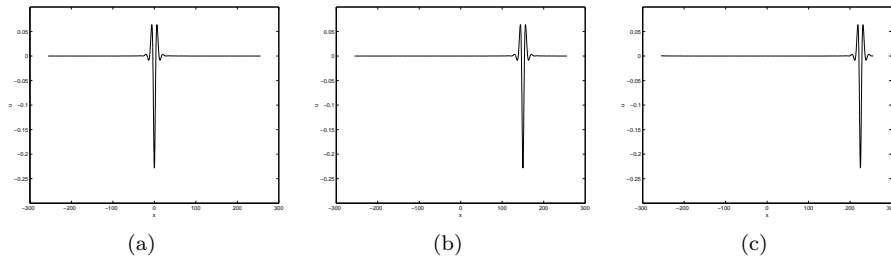
Figure 15: Numerical solution from the initial s-w profile for $\gamma = 0.9$: (a) $t = 0$; (b) $t = 200$; (c) $t = 300$.



(a)          (b)          (c)
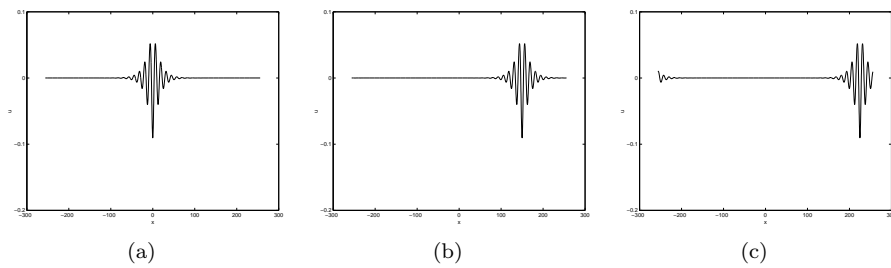
Figure 16: Numerical solution from the initial s-w profile for $\gamma = 0.99$: (a) $t = 0$; (b) $t = 200$; (c) $t = 300$.

24

provided in Figures 17, 18 and 19. They correspond to the previous figures, but here the waves at times $t = 200, 300$ have been magnified. In all cases, no spurious forward or backward oscillations are observed and the corresponding profiles propagate without any disturbances.
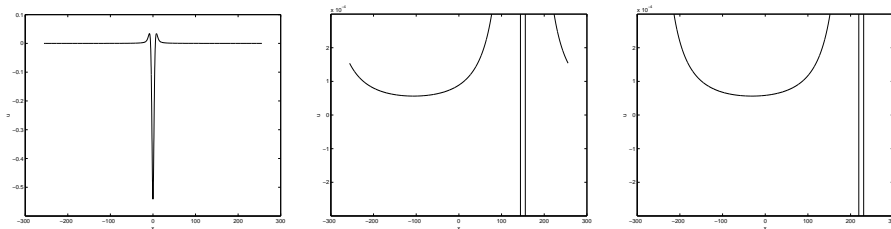


Figure 17: Magnification of Figure 14.
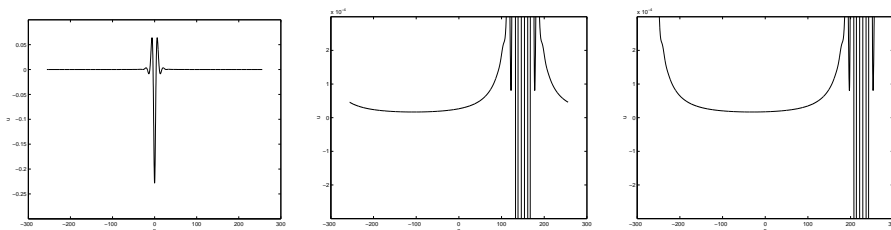


Figure 18: Magnification of Figure 15.

In order to assess the accuracy of the numerical travelling-wave solution we study its amplitude and speed. In Table 6, we show the minimum value of the initial profile, obtained by computing the minimum of the corresponding interpolating trigonometric polynomial. Table 6 has been used to generate Figure 20. Here, for each value of $\gamma$ (including the KdV case $\gamma = 0$), the initial amplitude has been compared with the corresponding amplitude (computed in the same way) of the numerical solution up to $t = 300$. For all $\gamma$, the amplitude error is of order of $10^{-9}$ and does not grow with time.

A similar study can be made for the speed. The initial profiles were all
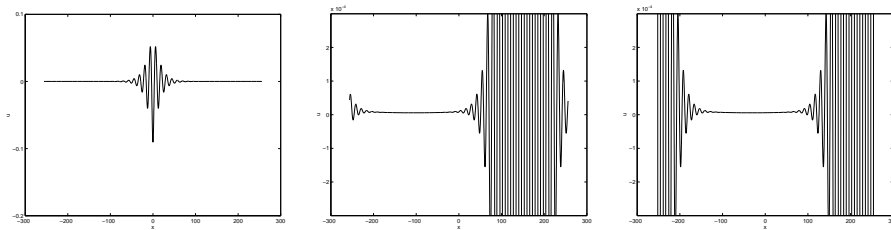


Figure 19: Magnification of Figure 16.

25

| $\gamma$ | Amplitude |
|---|---|
| 0 | $-0.75$ |
| 0.1 | $-7.183404555524147e - 001$ |
| 0.5 | $-5.411747962142054e - 001$ |
| 0.9 | $-2.280941079089593e - 001$ |
| 0.95 | $-1.656679129094486e - 001$ |
| 0.99 | $-9.035736815781438e - 002$ |

Table 6: Computed minimum of the initial solitary-wave profiles, for some values of $\gamma$.
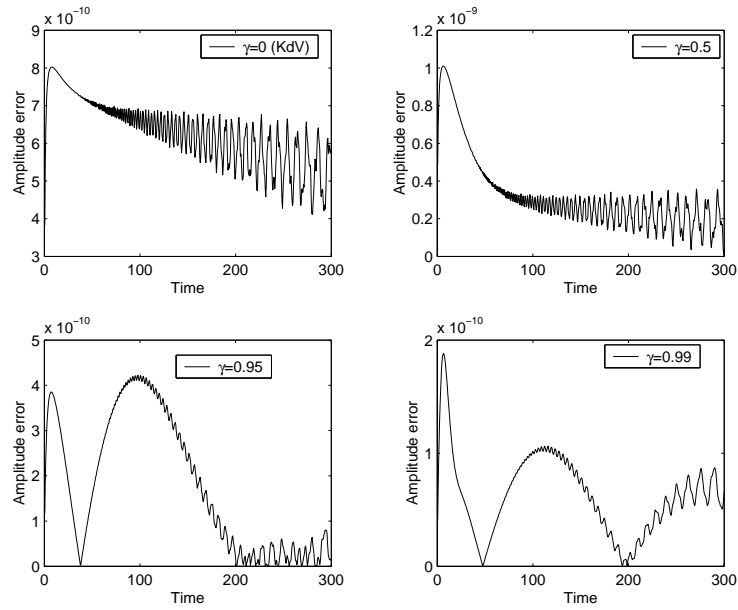


Figure 20: Temporal evolution of the error between the amplitude of the initial solitary-wave profile and of the evolving solution.
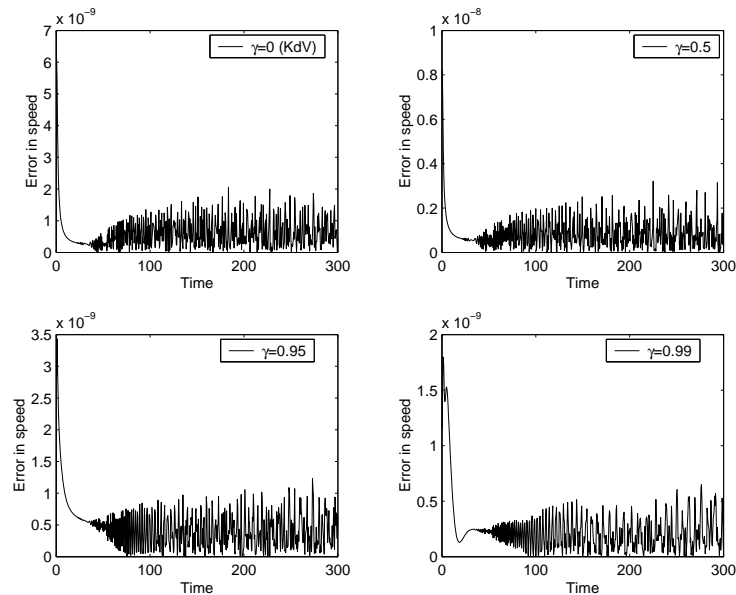
Figure 21: Temporal evolution of the error between the speed of the initial solitary-wave profile and of the evolving solution.

computed with a speed $c_s = 0.75$, which was the speed of reference to generate the errors observed in Figure 21. The speed of the travelling wave has been computed in the standard way, [13], by dividing the increment of the spatial translation of the center of the pulse over $\Delta t$ at each time step. The errors in the speed are also quite small and remain bounded. This and the previous figure suggest that the computed initial solitary-wave profiles are good approximations to the real ones and that the temporal discretization is accurate.

We have previously mentioned that the time integrator is not initially designed to preserve the discrete version of the Hamiltonian. In Figure 22, the evolution of the error between the values of $E_h$ of the numerical solution and of the initial profile up to $t = 300$ is displayed. The method virtually preserves the discrete Hamiltonian, which is also a suggestion of good approximation, since the integrator is only constructed to preserve the quadratic quantity $I_h$, [14].

The accuracy of the computed profiles is also reflected in the simulation of the multi-pulse waves. As an illustration, Figure 23 shows the evolution of a two-pulse solitary-wave profile, for $\gamma = 0.9$, at different times.

### Acknowledgements

27
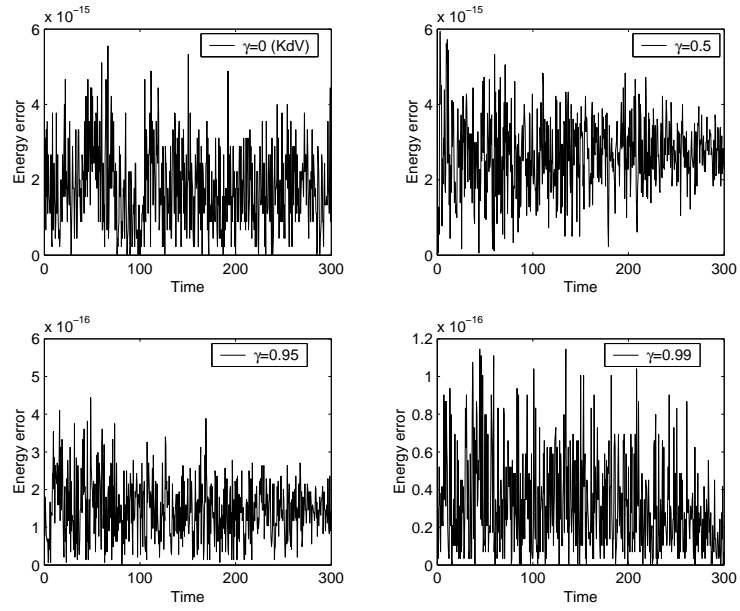
Figure 22: Temporal evolution of the error between $E_h$ of the initial solitary-wave profile and of the numerical solution.
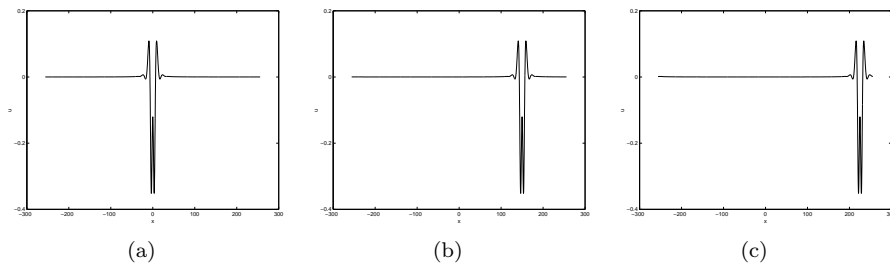


Figure 23: Numerical evolution from the initial two-pulse solitary-wave profile for $\gamma = 0.9$: (a) $t = 0$; (b) $t = 200$; (c) $t = 300$.

28

## References

[1] M.J. Ablowitz, Z.H. Musslimani, Spectral renormalization method for computing self-localized solutions to nonlinear systems, Opt. Lett. 30 (2005) 21402142.

[2] J. P. Albert, J. L. Bona, J. M. Restrepo. Solitary-wave solutions of the Benjamin equation, SIAM J. Appl. Math., 59 (1999) 2139-2161.

[3] W. Bao, Q. Du, Computing the ground state solution of Bose-Einstein condensates by a normalized gradient flow, SIAM J. Sci. Comput. 25(5) (2004) 1674-1697.

[4] T. B. Benjamin, Internal waves of permanent form in fluids of great depth, J. Fluid Mech. 29 (1967) 559-592.

[5] T. B. Benjamin. A new kind of solitary wave, J. Fluid Mech., 245 (1992) 401-411.

[6] T. B. Benjamin. Solitary and periodic waves of a new kind, Phil. Trans. R. Soc. Lond. A, 354 (1996) 1775-1806.

[7] J. L. Bona, M. Chen, A Boussinesq system for two-way propagation of nonlinear dispersive waves, Physica D, 116 (1998) 191-224.

[8] J. P. Boyd, Solitons from sine waves: analytical and numerical methods for non-integrable solitary and cnoidal waves, Physica D, 21 (1986) 227-246.

[9] J. P. Boyd, Chebyshev and Fourier Spectral Methods, 2nd ed. Dover Publications, New York, 2000.

[10] J.P. Boyd, Deleted residuals, the QR-factored Newton iteration, and other methods for formally overdetermined determinate discretizations of nonlinear eigenproblems for solitary, cnoidal, and shock waves, J. Comput. Phys. 179 (2002) 216237.

[11] J.P. Boyd, Why Newton's method is hard for travelling waves: small denominators, KAM theory, Arnold's linear Fourier problem, non-uniqueness, constraints and erratic failure, Math. Comput. Simul. 74 (2007) 72-81.

[12] M. Caliari, A. Ostermann, S. Rainer, M. Thalhammer, A minimisation approach for computing the ground state of Gross-Pitaevskii systems, J. Comp. Phys. 228(2000) 349-360.

[13] V. A. Dougalis, A. Durán, M. A. López-Marcos,D. Mitsotakis, A numerical study of the stability of solitary waves of the Bona-Smith family of Boussinesq systems, J. Nonlinear Sci. 17 (2007) 569-607.

[14] J. de Frutos, J. M. Sanz-Serna, Accuracy and conservation properties in numerical integration: the case of the Korteweg-de Vries equation, Numer. Math. 75(1997) 421-445.

[15] J.J. Garcia-Ripoll, V.M. Perez-Garcia, Optimizing Schrödinger functionals using Sobolev gradients: applications to quantum mechanics and nonlinear optics, SIAM J. Sci. Comput. 23 (2001) 1316-1334.

[16] G. Golub, C. Van Loan, Matrix Computations, third ed., The Johns Hopkins University Press, Baltimore, 1996.

[17] E. Hairer, C. Lubich and G. Wanner, Geometric Numerical Integration, Structure-Preserving Algorithms for Ordinary Differential Equations, Springer-Verlag, New York-Heidelberg-Berlin, 2002.

[18] E. Hairer, S. P. Norsett and G. Wanner, Solving Ordinary Differential equations I. Nonstiff Problems, 2nd ed. Springer Series in Computational Mathematics 8, Springer-Verlag, New York-Heidelberg-Berlin, 1993.

[19] H. Kalisch, J. L. Bona, Models for internal waves in deep water, Discret. Contin. Dyn. Syst. 6 (2000) 1-20.

[20] T. I. Lakoba and J. Yang, A generalized Petviashvili method for scalar and vector Hamiltonian equations with arbitrary form of nonlinearity, J. Comput. Phys. 226 (2007) 1668-1692.

[21] T.I. Lakoba, J. Yang, A mode elimination technique to improve convergence of iteration methods for finding solitary waves, J. Comp. Phys. 226 (2007) 16931709.

[22] F. Linares, M. Scialom, On generalized Benjamin type equations, Disc. Cont. Dyn. Syst. 12 (2005) 161-174.

[23] S. A. Martucci, Symmetric convolution and the discrete sine and cosine transforms, IEEE Trans. Signal Processing 42 (1994) 1038-1051.

[24] H. Olkkonen, P. Pesola, J. T. Olkkonen, Computation of Hilbert Transform via Discrete Cosine Transform, J. Signal Inform. Processing 1 (2010) 18-23.

[25] D. E. Pelinovsky and Y. A. Stepanyants, Convergence of Petviashvili's iteration method for numerical approximation of stationary solutions of nonlinear wave equations, SIAM J. Numer. Anal. 42 (2004) 1110-1127.

[26] V. I. Petviashvili Equation of an extraordinary soliton, Soviet J. Plasma Phys. 2 (1976) 257-258.

[27] W. C. Rheinboldt, Numerical continuation methods: a perspective, J. Comput. Appl. Math. 124 (2000) 229-244.

[28] G. Strang, The Discrete Cosine Transform, SIAM Rev. 41 (1999) 135-147.

[29] J. Yang, Newton-conjugate-gradient methods for solitary wave computations, J. Comput. Phys. 228 (2009), 7007-7024.

[30] J. Yang, Nonlinear Waves in Integrable and Nonintegrable Systems, SIAM, Philadelphia, 2010.

[31] J. Yang, T.I. Lakoba, Accelerated imaginary-time evolution methods for the computation of solitary waves, Stud. Appl. Math. 120 (2008) 265-292.

[32] J. Yang, T.I. Lakoba, Universally-convergent squared-operator iteration methods for solitary waves in general nonlinear wave equations, Stud. Appl. Math. 118 (2007) 153-197.

[33] J. Yang, B.A. Malomed, D.J. Kaup, Embedded solitons in second-harmonic-generating systems, Phys. Rev. Lett. 83 (1999) 1958-1961.